Tunable Metamaterials for Impact Mitigation

Lawrence Smith[a] *Brandon Hayes*[a] *Kurtis Ford*[b] *Elizabeth Smith*[b] *David Flores*[b] *Robert MacCurdy*[*a]

[a]University of Colorado Boulder
1111 Engineering Dr. UCB 427
Boulder, CO, USA, 80309

[b]Sandia National Laboratories
1515 Eubank Blvd SE
Albuquerque, NM 87123

*Corresponding Author Email Address: *maccurdy@colorado.edu*

Keywords: *Impact Mitigation; Additive Manufacturing; Computational Design; Metamaterials*

Abstract

Traditional methods of shielding fragile goods and human tissues from impact energy rely on isotropic foam materials. The mechanical properties of these foams are inferior to an emerging class of metamaterials called plate lattices, which have predominantly been fabricated in simple 2.5D geometries using conventional methods that constrain the feasible design space. In this work, we use additive manufacturing to relax these constraints and realize 3D plate lattice metamaterials with nontrivial, locally varying geometry. We circumvent the limitations of traditional computer aided design tools and allow the simulation of complex buckling and collapse behaviors without a manual meshing step. By validating these simulations against experimental data from tests on fabricated samples, we enable sweeping exploration of the plate lattice design space. Numerical and experimental tests demonstrate plate lattices absorb up to 6 times more impact energy at equivalent densities relative to foams and shield objects from impacts 10 times more energetic while transmitting equivalent peak stresses. In contrast to previous investigations of plate lattice metamaterials, we explore designs with nonuniform geometric prebuckling in the out of plane direction, and show that these designs exhibit 10% higher energy absorption efficiency on average, and 25% higher in the highest-performing design.

Data Availability

Constructive geometry design tools used to generate metamaterial geometry are freely available from https://github.com/MacCurdyLab/PlateLatticeMetamaterials, experimental data available upon request.

Funding and Permissions

This research is supported by a Sandia National Laboratories matching grant (AWD-23-03-0079) and by internal MACLab startup funds at the University of Colorado, Boulder.

Authors state no conflicts of interest.
No patient consent required for this research.
No clinical trial registration required for this research.
No ethics approval statement required for this research.
No permission for reproduction of material from other sources required for this research.

1 Introduction: Energy Absorption

Stochastic cellular materials are ubiquitous in energy absorption, vibration isolation, and shock mitigation applications. Introducing voids into a solid material reduces the relative density and can adjust the mechanical properties by a factor of 1000 or more from those of the constituent material [1], yielding improved energy absorption performance (Figure 1A). By choosing a base material and controlling process parameters that govern the average pore size, designers exert rudimentary control (Figure 1B) over the macroscale mechanical properties of the resulting metamaterial, which tend to scale with relative density ρ^* ($n \in [1, 4]$):

$$\frac{\text{macroscale cellular solid property}}{\text{base material property}} \propto (\rho^*)^n \tag{1}$$

Yet the popularity of foams in impact absorption applications is pragmatic (they are inexpensive, volume-filling, and isotropic), not due to optimal performance. To date, no foam material has been demonstrated which outperforms architected (non-stochastic) materials on a specific modulus, toughness, or energy absorption basis [2]. Designers cannot directly prescribe the microscale geometry of foam materials; stochastic physical processes like bubble nucleation, cell growth, and phase change separate their design intentions from resulting microscale geometry. Although extensive experimental and analytical work has been dedicated to understand the scaling behavior and performance bounds on foamed materials, their performance remains sensitive to manufacturing details [3].

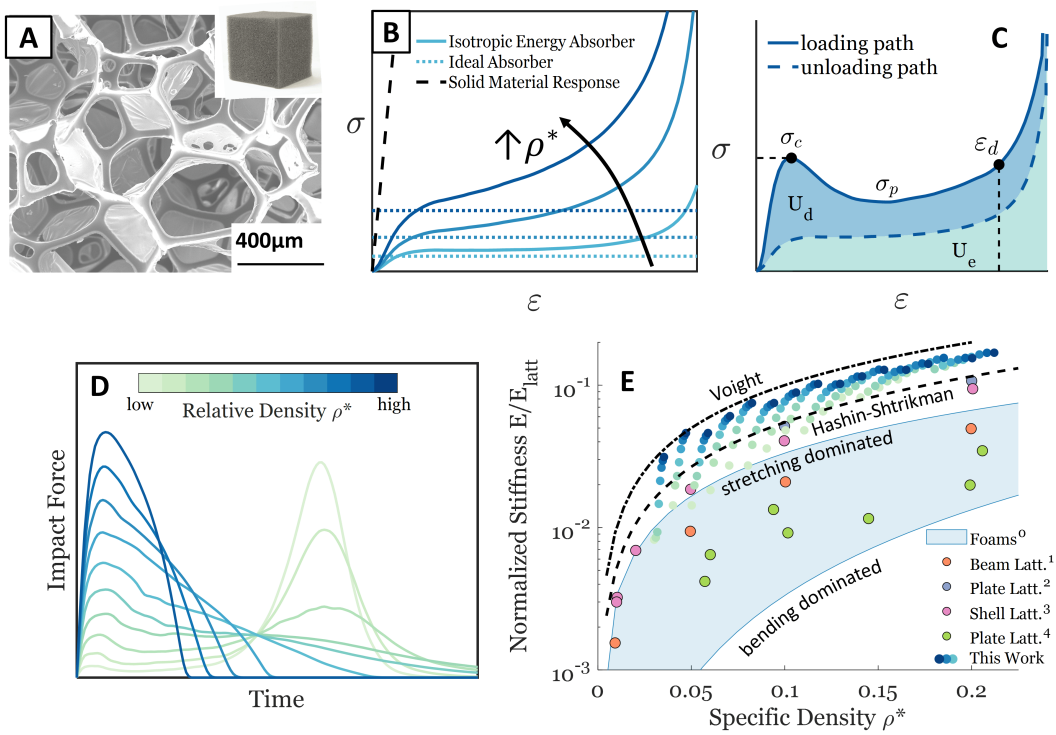

Figure 1: Designers of stochastic foam energy absorbers (e.g. polyurethane foam micrograph, A) exert only rudimentary control over stress strain response via adjustment of relative density and choice of base material (B). These foamed materials collapse at a near-constant stress over a wide range of strains, allowing high energy absorption without transmitting high forces. Beyond a critical specific impact energy absorbed, the materials undergo densification (C, at ε_d) and force transmission is extremely sensitive to additional strain. Dynamic simulations of isotropic foam impact samples with increasing density (D) reveal the importance of matching specific impact energy absorbed before reaching densification strain ε_d to specific impact energy. Soft foam materials absorb insufficient energy before densifying, and subsequently transfer large forces, while stiff foam materials absorb impact energy with increasingly higher forces and lower deformation. By sacrificing the isotropy of stochastic materials, architected materials with outstanding stiffness in a single direction can be achieved (E). Foam micrograph in A was taken using a Hitachi SU3500 scanning electron microscope (SEM) with an acceleration voltage of 15 kV. SEM support was provided by the Colorado Shared Instrumentation in Nanofabrication and Characterization facility (University of Colorado Boulder).

Unlike the design of other metamaterials (e.g. minimally compliant materials), energy absorptive materials must simultaneously balance several performance criteria to provide useful protection [4]. High performance designs absorb the kinetic energy of a particular impact scenario while limiting peak loads transferred to protected objects [5]. This cannot be achieved by materials at upper or lower limits of specific stiffness or strength (Figure 1C). In fact, the stress/strain response of a theoretical ideal absorber [6] is necessarily linked to a particular impact energy and compression distance at hand, and compresses that entire distance at a constant force such that the integral $\int Fdx$ exactly totals the input energy. The practical design and use of foams remains an experimental exploration of base material selection on the one hand, and process parameters that underdetermine microscale geometry on the other [7].

Additive manufacturing (AM) offers a promising alternative to this paradigm. By controlling the deposition of build material at resolutions separated by four orders of magnitude from the build volume, it is possible to create metamaterials with deterministic, fully controlled geometry across multiple length scales. Additionally, sample geometry can be locally or directionally tailored, enabling region-specific and functionally graded mechanical properties. This level of control over local mechanical properties is not a hallmark of working with foam materials [8, 9]. Finally, advanced AM technolgoies can co-print with multiple distinct base materials of widely varying mechanical properties [10]. Taken together, AM enhances design freedom and flexibility, and enables searches over microstructure geometry *and* material composition in pursuit of higher performance metamaterials.

In this work we investigate the quasistatic response and dynamic impact performance of locally tunable elastomeric plate lattice (PL) materials (Figure 2A). In contrast to previous work, we demonstrate high-performance designs with graded geometric prebuckling in the out-of-plane direction (which is the extruded direction of a honeycomb with no prebuckling), and we compare impact performance directly to baseline foam-like materials. We use an efficient, fully scripted geometry generation and simulation pipeline to explore the plate lattice design space and impact test gamut more widely than is possible via experimental testing alone. Our method allows for the broadest characterization of plate lattice impact performance to date, demonstrating that these materials offer exceptional properties relative to industry-standard stochastic foams: they absorb 6 times more energy at equivalent density and up to 10 times more energy while transmitting equivalent peak forces. Plate lattice designs with nonuniform geometric prebuckling, which are investigated for the first time in this work, absorb 22% more energy and exhibit 10% higher energy absorption efficiency on average than uniform designs similar to those investigated in previous work. To quantify real-world impact mitigation (where precise loading conditions are unknown), we quantify the performance *bandwidth* of energy absorbers - the range of specific impact energies over which designs effectively mitigate impact force transmission. Plate lattice metamaterials transmit near-constant peak stresses across the full range of impact energies explored experimentally, demonstrating robust performance relative to reference foams. Our investigation focuses on metamaterial *geometry* and not on base material selection; we expect the results described here to translate to a variety of AM technologies and materials.

1.1 Background: Energy Absorbing Materials

Exhaustive experimental characterization of energy absorbing metamaterials has been performed and aggregated into review articles; some 80 such results are referenced across [4], [7], and [11] alone. The field is increasingly focused on the design and characterization of periodic, strut-based structures unlocked by recent advancements in AM; widely-known octet truss lattices were immediately shown to exceed specific strength, stiffness, and energy absorption properties of stochastic materials [12, 13, 14]. Still-higher performance has been achieved by plate lattices, which are conceptually similar to their strut counterparts: a set of nodal points is connected by high-aspect ratio structural members, sometimes in a repeating pattern. Bonatti and Mohr find that plate lattices provide substantially higher stiffness and strength than optimal truss-lattices of equal mass using analytical techniques and several hundred finite element simulations [15], a result that holds under high strainrate testing [16]. Mohr investigates lattices derived

from the shear planes of crystal systems; these materials achieve the theoretical Hashin-Schtrickman bounds on modulus and the Suquet bounds on strength for isotropic cellular solids [17, 18]. Related work extends this investigation to minimum curvature periodic shell lattices, including under large strains and impact loading [19, 20]. Comparisons between analytical, numerical, and experimental results for energy absorption and strength in quasistatic compression of ultralight ($\rho^* = 0.01$) metamaterials based on hollow truss lattices [21] and minimal surfaces [22] have shown similarly high specific strength. Interestingly, simulations in this work identify optimal geometries with nonuniform wall thickness, which were never physically realized due to constraints on the nickel coating and etching fabrication process implemented.

This points to another design principle emerging from various works on AM metamaterials: nonuniform, locally tuned, or graded geometric properties are generally advantageous in energy absorption. Early work in the response of nonuniform strut lattices with quasistatic and impact loading indicates up to a 45% increase in specific impact energy absorption relative to uniform samples [23]. A detailed examination of the progressive collapse behavior of similar functionally graded lattices shows density grading can prevent undesirable diagonal shear banding behavior, leading to more repeatable energy absorption than constant-density counterparts [24]. In a study of in-plane compression of hexagonal honeycomb structures, graded designs densify at larger strains than uniform-density samples and exhibit improved energy absorption [25].

Finally, to push metamaterial energy absorption performance beyond even the theoretical limits for isotropic cellular solids, we reexamine the prioritization of mechanical isotropy that runs throughout the results discussed thus far. If the direction of an impact load is known *a priori*, we can prioritize optimization of mechanical properties in that direction - an approach exemplified in structural honeycomb metamaterials widely used in aerospace, automobile, railway, and packaging applications. Many previous efforts have characterized honeycomb structures in out of plane compression and shear using experimental [26, 27] and numerical [28, 29] methods. These have an analytically predicted a sevenfold increase in collapse stress [5] and experimentally demonstrated a fourfold increase in plateau stress [30] over isotropic foams of equivalent relative density.

1.2 Quantifying Impact Energy Absorption Performance

Investigation into energy absorptive materials is conducted via distinct experimental methods, depending on the strain rates of interest. Load frames are capable of prescribing quasistatic to moderately dynamic ($10^{-5} - 10^{1} s^{-1}$) strain rates $\dot{\varepsilon}$ with high precision, and are used to study energy absorption in compression for metallic [4, 15, 31, 32, 33], elastomeric [34, 35], and polymeric [7, 36, 37] materials. For higher ($10^{1} - 10^{4} s^{-1}$) strain rates, researchers use impact tests; impact energy is prescribed by controlling the mass and impact velocity of the impacting object. Typical outputs from these experiments include force/acceleration profiles and measurements of dissipated energy.

Less research effort has been devoted to exploring rate-dependent energy absorptive properties of materials compared to quasi-static material properties [38], but existing studies point to strong strain-rate sensitivity in deformation behavior for both elastomeric [39] and elastic-plastic [40] metamaterials. Song et al. investigate rigid polyurethane [37] and glass microsphere-doped epoxy [41] foams under quasistatic and high-strain rate compression (10^{-4} - $10^{3} s^{-1}$), and report increases in modulus and yield strength with strain rate. In an example of impact and geometry-specific experimental testing, DeMarco [42] reports acceleration profiles and dissipation values for motorcycle helmets impacting a steel anvil.

1.3 Material Selection for Energy Absorbers

New research into the impact performance of architected cellular structures constructed from soft elastomeric materials [34] shows their promise in everyday applications. These materials exhibit glass transi-

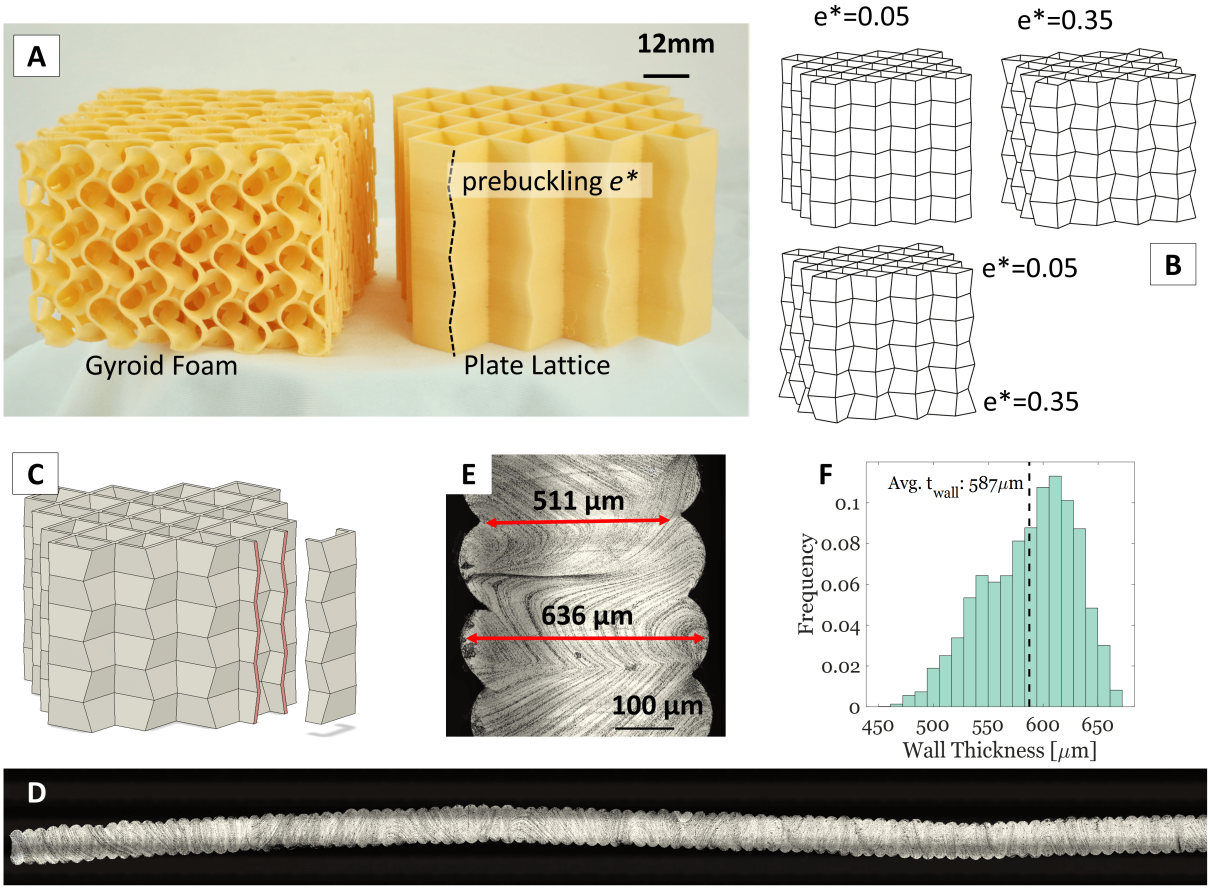

Figure 2: Typical samples fabricated via additive manufacturing for experimental testing in quasistatic and dynamic compression. A shows plate lattice sample and equivalent-density TMPS gyroid foam used as reference, while B shows effects of adjusting geometric prebuckling parameter e^* on a global (upper) and local (lower) scale. Plate lattices are printed at the lower limit of resolution of commodity additive manufacturing hardware, with the wall thickness created by a single pass of the $0.4mm$ orifice nozzle. A Keyence VK X-1100 profilometer is used to scan a section cut (C) through a manufactured sample, producing a high-resolution stitched image (D). A custom algorithm is used to compensate for wall eccentricity and gather 2500 measurements of wall thickness, which shows periodic variation in the z direction due to print layer lines (E). Mean wall thickness is $587 \pm 40\mu m$ at one standard deviation, slightly below the design thickness of $600\mu m$ (F).

tion temperatures far below ambient conditions and support high strains without fracture or yield, meaning that deformations are highly reversible and structures may absorb many repeated impacts [43]. Additionally, experimental investigation of shock propagation through buckling elastomeric metastructures [44] reveals that high-strain rate impacts can activate deformation modes not induced by quasistatic loading, which reduce force transmission through a sample under test. This work exemplifies how designers can exert substantial control over impulse response via selection of geometric and material parameters, and that understanding impact performance of viscoelastic metamaterials requires consideration of their dynamic stability and loading rate.

AM allows designers to exercise even more design freedom, enabling higher tunability in material response than is possible in stochastic materials [39, 44]. Townsend et al. [34] investigate the quasistatic compression of pleated honeycomb structures, demonstrating specific impact energy absorption properties that rival polymeric foams while offering higher design flexibility - specifically, continuous control over undesirable stress softening behavior typical of honeycomb structures. The authors extend this work [45] to investigate the energy absorption behavior of pre-deformed hollow cylindrical structures in quasistatic and impact loading. Related efforts use AM to realize bistable metamaterials capable of "trapping" impact energy via tightly controlled geometry, a response not seen in any natural materials [46]. Liquid crystal elastomers (LCEs), which undergo mechanically-induced, energy-dissipating phase transition under large strains, have recently been explored as AM base materials for energy absorption

[47].

2 Results

2.1 Plate Lattice Metamaterials

In this work we adopt a modified version of a plate lattice introduced by [34], which features repeated quadrilateral plates and a spatially-varying prebuckling parameter used to control macroscale compression behavior. To avoid bottlenecks and limitations of traditional Computer Aided Design (CAD) tools, we implement a custom constructive geometry code which produces plate lattice geometries to designers' specifications. With a single click the tool automatically produces a computational mesh of the design suitable for finite element analysis *and* a fabrication file ready for additive manufacturing (Figure 2A); the generation of these representations is typically a time- and labor-intensive manual process (tool available from https://github.com/MacCurdyLab/PlateLatticeAnalysis).

Using this tool, node locations can be freely adjusted on a local basis while preserving node connectivity, unlocking a wealth of plate lattice geometries not previously explored, including those with nonuniform wall thickness, spatially-varying prebuckling parameter, and nonuniform cell sizes. A prebuckling parameter $e^*(x, y, z)$ that is a function of space is defined to control the local eccentricity of the lattice; increasing e^* skews nodal positions about the cell vertical centerline while the lattice approaches a honeycomb material as $e^* \to 0$ (Figure 2B). The design space parameterization used in the remainder of this work, along with typical parameter values, is given in Table 1.

Table 1: Design Parameterization & Typical Values

Parameter	Variable	Typical Value
Number of Unit Cells	$[n_x\ n_y\ n_z]$	[4 4 6]
Unit Cell Height	h_c	$8mm$
Unit Cell Length	w_c	$12mm$
Wall Thickness	t_{wall}	$0.6mm$
Geometric Prebuckling	e^*	0.05-0.25

Plate lattices fabricated via fused deposition modeling additive manufacturing technology closely resemble designed geometry, achieving sub-$1mm$ wall thickness throughout a sample with exterior dimensions $64{\times}64{\times}48mm^3$. Plate latices are printed with wall thicknesses at the lower resolution limit of the printer hardware, so cross-section analysis was performed to quantify deviations from the design dimensions. Samples are sectioned through the vertical wall with a razor blade (Figure 2C) and imaged using a Keyence VK X-1100 optical profilometer (Figure 2D,E). Taking 2500 optical measurements over half the height of the plate lattice, a mean wall thickness of $587\pm 40\mu$m was determined, slightly below the design wall thickness of 600μm. Local measurements mirror the "rectified sine wave" profile expected in an extruded-filament based AM (Figure 2E,F). In subsequent finite element simulations of plate lattice behavior, this geometry is approximated as uniform thickness equal to the mean value of 587μm.

In order to establish a reference material to compare against the performance of plate lattice materials, control samples with gyroid triply periodic minimal surface (TPMS) geometry[48] were fabricated for experimental testing. Owing to their ease of design and fabrication, these structures are well-characterized in the literature, and have been shown to mimic the performance of isotropic foam materials when fabricated from metals, plastics, and elastomers [36]. In this work, gyroid structures are fabricated using the same base material and print settings as plate lattices, and are printed to identical external dimensions and volume density, ensuring that any differences in impact absorption performance can be attributed to the geometry of the samples. These samples permit direct experimental comparison between novel anisotropic plate lattice designs and traditional isotropic foam-like materials in impact conditions, which is absent from previous investigations of plate lattice behavior [45, 34].

2.2 Metamaterial Constitutive Response

We characterize the mechanical response to compression loading in plate lattice materials by mapping the stress-strain response of various geometries using experimental and numerical methods. For the remainder of this document, we use the symbols σ and ε to refer to stress and strain values computed over the full sample geometry; σ is computed by dividing compressive force by projected area and ε is computed by dividing compression distance by undeformed sample height. Relative to reference foams, plate lattice materials exhibit pronounced differences in response to compression, including higher initial stiffness and higher stress plateaus at equivalent density (Figure 3A), resulting in up to 6× increase in useful energy absorbed [12] and higher energy absorption efficiency E^* (Figure 3B):

$$E^*(\varepsilon) = \frac{\int_0^{\varepsilon} \sigma d\varepsilon}{max(\sigma(\varepsilon))} \tag{2}$$

where σ and ε indicate compressive lattice stress and strain, respectively. As indicated by three reference foams plotted in Figure 3A, modifying the relative density of a foam sample is the only means by which designers can exert control over the base-material's mechanical response; increasing the relative density raises, shortens, and pitches the stress plateau upward, resulting in lower peak efficiency.

Excellent agreement between simulated and experimental results is achieved in quasistatic compression tests across various geometries, allowing us to leverage numerical models to explore a wider range of wall thicknesses and prebuckling parameters than was possible to test in experiment (Figure 3C). We find an average error between mean experimental response and simulated response below 10% across the entire range of strains in all quasistatic simulations, which feature complex geometric and material nonlinearities, self contact, and frictional interaction.

Plate lattices with minimal prebuckling ($e^* \rightarrow 0$) exhibit an initial peak in the stress strain response (Figure 3A) associated with the onset of localized buckling and subsequent geometric softening, after which plate members are loaded in bending rather than stretching. This effect can be mitigated by increasing the geometric prebuckling factor, which makes this peak less pronounced at the cost of simultaneously lowering the plateau stress. This density-independent, continuously tunable parameter enables precise matching of plateau stress of a plate lattice material to a high-level requirement on acceleration for a particular impact scenario without impacting the densification strain.

Increasing geometric prebuckling e^* lowers the stress at which the lattice material is most efficient (highest E^*), but the value of that efficiency remains higher than for the reference foams tested (Figure 3B). Efficiencies predicted by quasistatic finite element simulations are near to but uniformly lower than those computed from quasistatic experimental data. This can likely be attributed to over-estimation of collapse stress σ_c or plateau stress σ_p by finite element simulations. Additional possible sources of simulation error include elastic anisotropy in 3D printed samples which is not reflected in the simulation's constitutive model, and deviations from the perfectly uniform as-designed geometry in 3D printed samples. Simulations of plate lattice compression with a variety of prebuckling level and wall thicknesses indicate that designs with $E^* > 0.4$ can be found across all relative densities tested, $\rho^* \in [0.02, 0.22]$ (Figure 3D).

2.3 Impact Performance

Impact testing remains the most reliable means of understanding the performance of impact absorbing materials in conditions that closely mimic practical use cases. It is well known that the macroscale stress-strain response of metamaterials made from a variety of base materials is strainrate-dependent [41, 44]. Our fabricated samples show rate-dependent macroscale response over two orders of magnitude variation on loading rate (Figure 3E,F). Characteristic stress/strain response remains consistent across the range of tested strain rates, including a sharp increase and local maximum followed by a long and flat stress plateau. Foam materials of various densities exhibit similar, but less pronounced changes (97% increase in stress plateau versus 140% change for PL), though being made of the same material and having

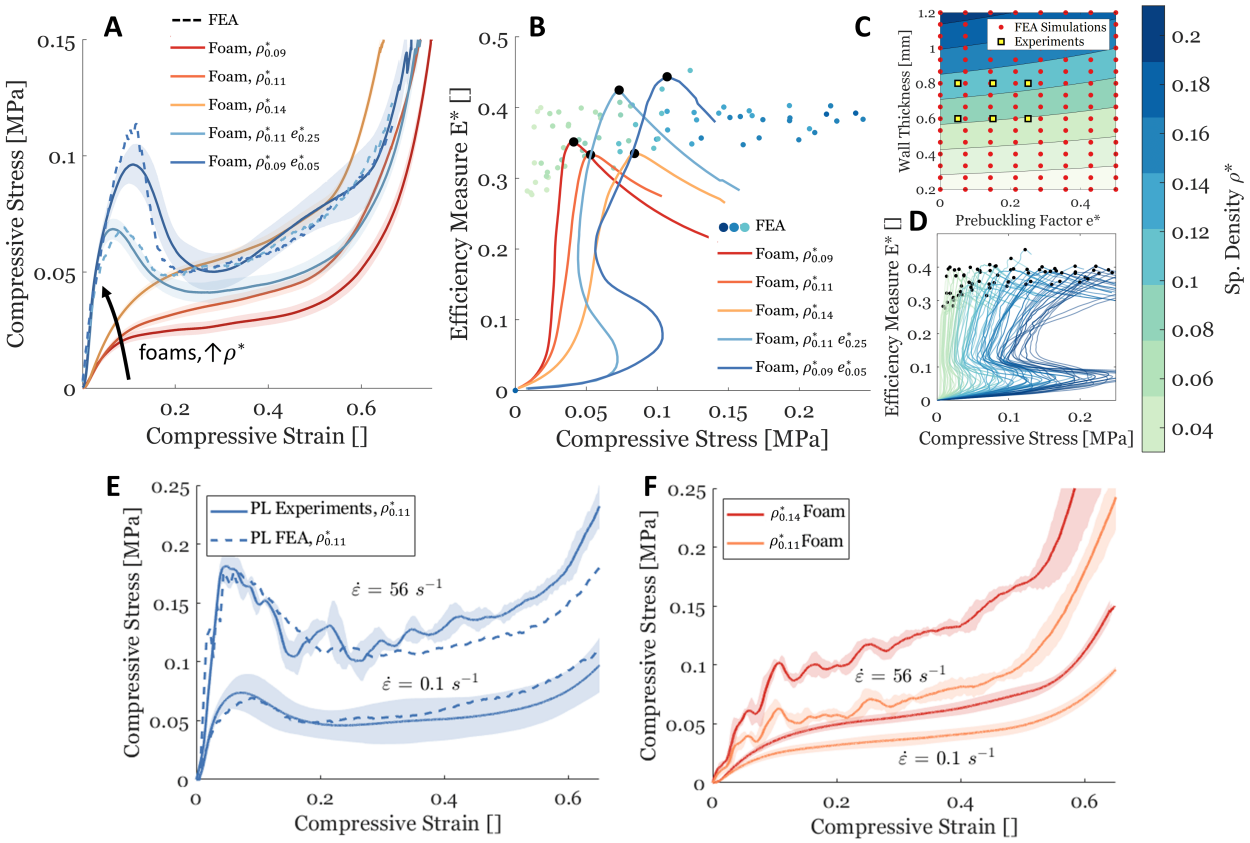

Figure 3: Quasistatic experiments indicate that plate lattice materials exhibit pronounced differences in macroscale stress/strain response relative to isotropic foam materials of similar relative densities, resulting in improved impact absorption performance. Adjustment of geometric prebuckling parameter e^* affords density-independent control of peak stress and stress plateau magnitude (A), while leaving densification strain unaffected (subscripts on ρ^* indicate relative density). All experimental tests are performed 8 times (twice on each of four replicates); centerline shows mean response while shaded region shows 2σ confidence bounds. Simulation results for analogous plate lattice tests agree with experimental data; this indicates that these models may be used to predict behavior of plate lattices with varied densities and prebuckling magnitude. Not only do plate lattice samples show a 28% average increase in efficiency (B, black points mark peak efficiency), the efficiency peaks are less pronounced, indicating less dramatic falloff in efficiency when subjected to variations in impact stress. Simulations across a wide range of plate lattice geometries (C) show that high-efficiency designs are obtained across a wide range of impact stresses (these efficiency peaks are indicated by points colored by density in B; full responses are given in D). Colorbar is shared by B,C, and D. Plate lattice stress response character remains consistent across the range of tested strain rates (2 orders of magnitude, E), including a sharp increase and local maximum followed by a long and flat plateau. Foam materials of various densities exhibit similar, but less pronounced changes, despite identical constitutive material and specific density (F).

similar specific density. Simulations indicate a possible explanation: plate lattices feature highly nonuniform strainrate fields. Thus peak local strainrates for plate lattices exceed those of foams even for identical $\dot{\varepsilon}$ and excite higher frequency components of the material's viscoelastic (strainrate-stiffening) response. Simulations of impact produce stress/strain responses very similar to those measured in experiments (Figure 3E), lending credibility to the dynamic finite element model. Oscillations in force signals are apparent in all our impact experiments, which manifest as oscillations in stress/strain responses (Figure 3E,F) in both plate lattice and gyroid foam materials. Investigation of high speed video indicates this phenomenon is linked to test fixture vibration. We note that other experimental investigations of transient force signals during impact (e.g. [45]) show vibration effects, even when using high-end commercial impact test equipment; mitigating these vibrations remains an open research topic [49].

Experimental and numerical results support the favorable performance of plate lattice materials relative to reference foam materials on the basis of specific impact energy absorption, prevention of impact load transmission, useful energy bandwidth, and energy dissipation. Figure 4A shows a representative experimental impact test conducted on plate lattice and reference foam samples with identical impact mass, impact velocity, sample volume, sample density, and constitutive material. Energy absorbed early in

the plate lattice compression (blue) prevents the sample from reaching full densification and limits peak forces reacted by a factor of 3.5 relative to foam sample (orange). High-speed video of this impact test is available in Supplementary Information. Simulation of impact tests on the plate lattice geometries tested in experiment (Figure 4B) allows us to analyze their performance across a wide range of impact energies beyond the capabilities of the test apparatus designed for this work. Figure 4C shows the peak impact stress reacted by reference foam materials and plate lattices with identical specific density. The foam material densifies across all impact energies tested, so the peak force transmitted is dominated by the material's bulk modulus and scales approximately linearly with increasing specific impact energy. In contrast, plate lattice materials show remarkable robustness to increasing impact energy, and transmit a relatively constant peak load across the range of energies tested. Analytical treatment of stretching- and bending-dominated foams [1] (see Supplementary Information for derivation) suggests that an analogous range of impact energies over which foams offer robust performance exists ($125 J/kg$ for this material and relative density), but this is below the lower limit of specific impact energy attainable by our test appa-

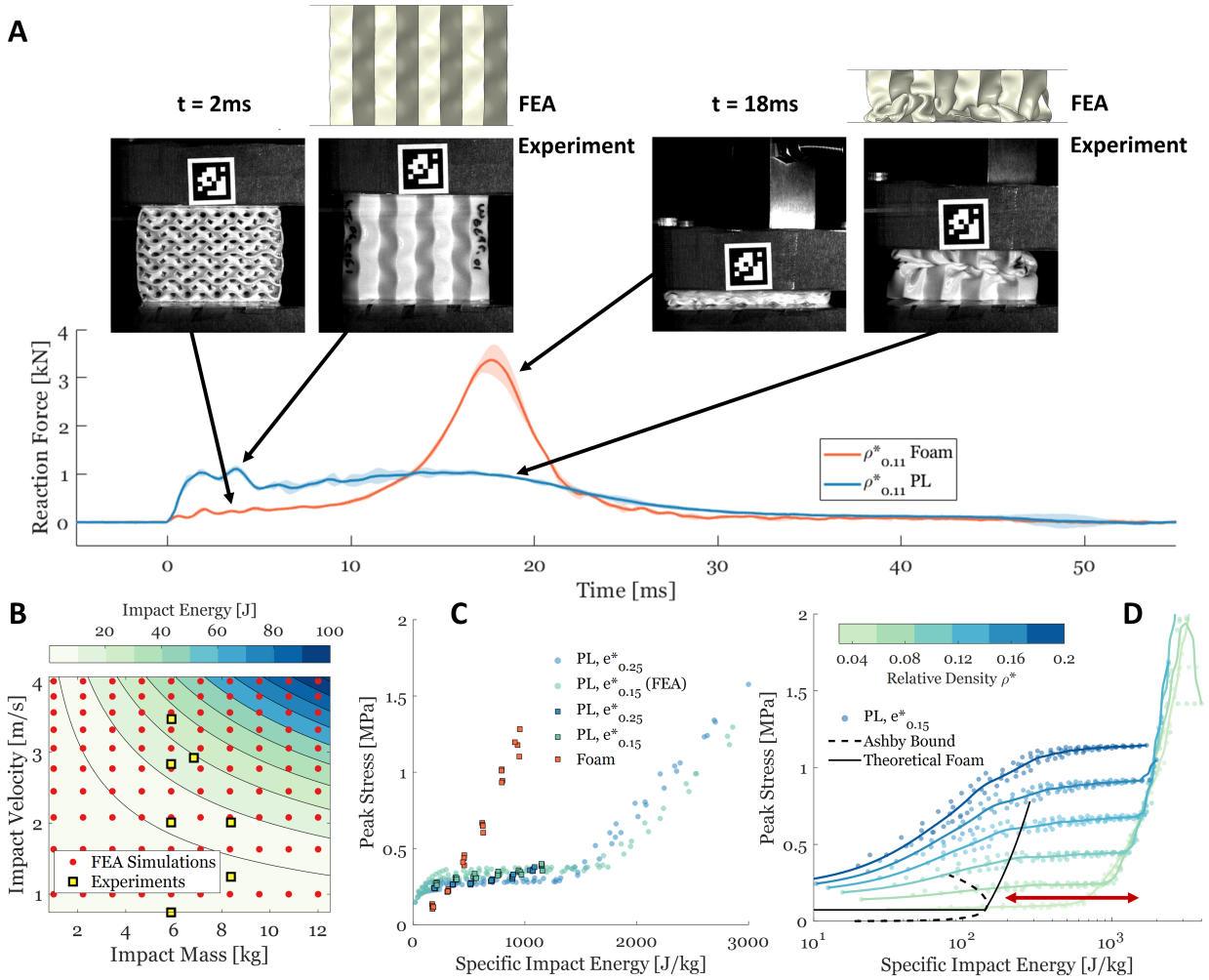

Figure 4: In impact experiments on a plate lattice sample (blue) and reference foam sample (orange) with identical mass, volume, base material, impact mass, and impact velocity, plate lattices control transmitted loads effectively by avoiding densification (A; subscripts on ρ^* indicate relative density). All experimental tests (B, square marks) are performed twice on each of four replicates; centerline shows mean response while shaded region shows 2σ confidence bounds. This peak reaction force transmitted by plate lattices is insensitive to increasing impact energy across the range tested in experiment (C, square marks), and simulated impacts across a wider range of energies indicate that plate lattices offer robust performance to even higher specific impact energies (C, circular marks) before densification occurs (knee point at $1500 J/kg$). Simulations of each of the 100 impacts in B across a slew of plate lattices with $\rho^* \in [0.020.22]$ indicate that this trend holds across a wider range of relative densities than was accessible in experiment: a relatively constant stress is transmitted over several orders of magnitude of impact energy (envelope bounded by the post-densification response in D, derivation included in Supporting Information). An analogous envelope of peak stress transmitted before densification for foams with $\rho^* \in [0.01, 0.50]$ is derived analytically (dashed line in D), with the response of a representative foam sample ($\rho^* = 0.11$) indicated by a solid black line. Plate lattice of equivalent density absorbs $10\times$ higher energy before densifying (indicated by red arrow).

ratus. Simulations of 100 impacts that include specific impact energy values extending beyond the limits of the impact test apparatus are aligned with experimental results (Figure 4C) where the specific impact energy was experimentally achievable. Beyond a critical impact energy U_{crit}^{-}, an energy absorber densifies and becomes highly sensitive to variations in impact energy - simulations indicate that this critical value for the plate lattices tested is approximately $1500 J/kg$ (the inflection point in Figure 4C), $10\times$ higher than reference foams at equivalent density and base-material.

To explore the performance bandwidth of plate lattice materials more thoroughly, an additional 800 simulated impact tests are performed on plate lattice materials with relative density ρ^* ranging from 0.02 to 0.22 (Figure 4D). These simulations illustrate a relationship between plate lattice density ρ^*, the peak stress reacted during impact, and the range of specific impact energies over which a plate lattice effectively controls impact loads (the energy absorption bandwidth). First, the peak stress reacted during each impact that is less energetic than U_{crit}^{-} scales linearly with increasing density. Second, as ρ^* increases, densification strain decreases - this manifests as a reduction in bandwidth at higher relative densities. Third, simulated plate lattice performance bandwidth is much higher than that of reference isotropic foams when compared across equivalent peak stress transmitted. We derive a relationship between specific impact energy and peak force transmitted using equations in [1] (see Supplemental Material) for stretch-dominated isotropic stochastic foams that collapse via elastic buckling, allowing us to identify U_{crit}^{-} for relative densities ranging from 1% to 50% (plotted with black dashes in Figure 4D). The response of one such foam with specific density $\rho^* = 0.20$ is predicted analytically and indicated by a solid line in Figure 4D.

Plate lattices with nonuniform geometric prebuckling in the out-of-plane direction, demonstrate higher energy absorption efficiency than their uniform prebuckling counterparts when simulated in realistic impact conditions. To demonstrate this effect, we perform two full factorial sweeps over two plate lattice design dimensions using our design and simulation pipeline: relative density ρ^* and geometric prebuckling magnitude. In the first sweep, geometric prebuckling is globally uniform (see Figure 2B, upper), which is consistent with previous investigations[45, 34]. In the second sweep, geometric prebuckling is graded as a function of the height of the sample (increasing from top to bottom, see Figure 2B lower), between $e^* = 0.05$ and a higher value such that the average geometric prebuckling through the height of the sample is identical to the corresponding design in the first sweep. Results from these 162 impact simulations demonstrate that spatially-varying geometric prebuckling e^* improves energy absorption ef-

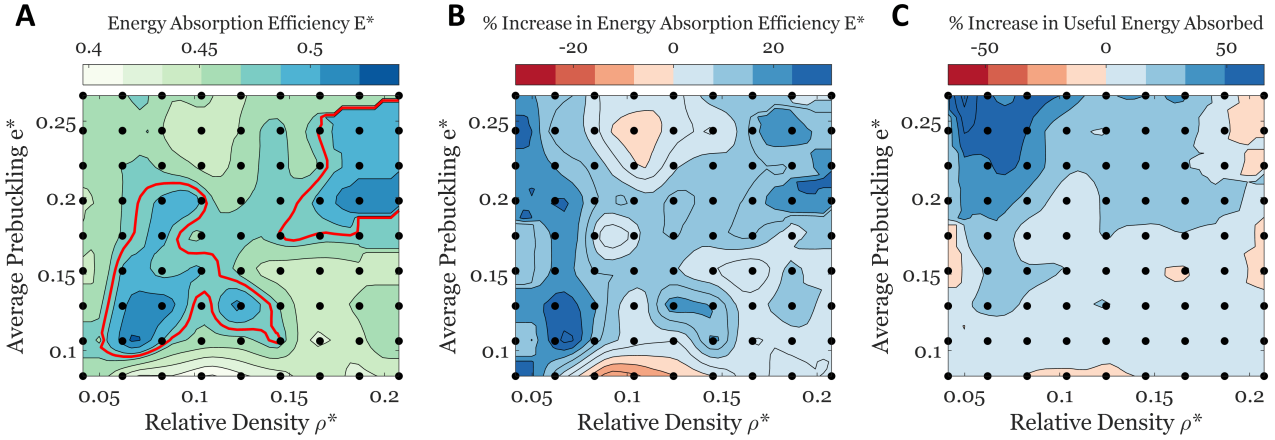

Figure 5: A full-factorial sweep over plate lattice specific density ρ^* and geometric prebuckling e^* magnitude demonstrate the advantages of designs with nonuniform prebuckling (A). We grade e^* in the loading direction and perform simulated impact tests. Peak energy absorption efficiency E^* is displayed in color contours (e^* averaged through the height of the sample is given on the vertical axis), with natural neighbor interpolation used to compute values between discrete sample points. The highest E^* reported in any similar work [35] is indicated by a red contour at $E^* = 0.49$. We compare the impact absorption efficiency of these plate lattices with graded e^* against their constant-e^* counterparts in B, showing up to 25% increase in E^* (mean E^* increase is 10%). Graded plate lattices absorb up to 80% (22% on average) more useful energy (energy absorbed up until the point of densification) than their uniform counterparts (C).

ficiency E^* relative to uniform samples with *identical* average e^*. Figure 5A displays E^* for a range of spatially-varying plate lattice designs using color contours; the highest E^* reported in any similar work ($E^* = 0.49$, [35]) is displayed using a solid red contour line. Natural neighbor interpolation is used to compute data between discrete points sampled in simulation sweeps. Figure 5B quantifies improvement in E^* for graded plate lattices relative to their uniform counterparts; the addition of graded e^* leads to an average 10% increase relative samples with uniform prebuckling, with maximum improvement over all geometries tested reaching 25%. In these simulations, impact velocity and mass are chosen to guarantee densification during the sweep on a per-design basis using relationships developed in previous parameter explorations. Energy absorbed up to the point of densification ε_d is useful for impact mitigation, as transmitted forces are effectively controlled in this regime. These simulations indicate that graded plate lattices absorb up to 80% (22% on average) more useful energy than their uniform counterparts (Figure 5C) at equivalent density and average prebuckling magnitude. We note that across 93% of the design space explored in this full factorial sweep, graded plate lattice designs absorb more useful energy than their uniform counterparts.

2.4 Energy Dissipation

While proper selection of base material and plate lattice geometry can effectively limit the transfer of high forces by increasing the duration of the impact even in a perfectly elastic scenario, in practice energy dissipation can be advantageous in limiting the rebound of protected objects following impact. Common dissipation mechanisms include material viscoelasticity, plasticity, phase change [47], and incidental or deliberate frictional interactions [50]. For plate lattice and reference foam samples studied here, energy is dissipated via the viscoelastic behavior of the constituent TPU material.
We first assess plate lattice dissipation and response to repeated loading via quasistatic cyclic compression tests, which indicate significant softening (Figure 6A) over 1000 load/unload cycles. The normalized dissipated energy drops to 25% of its initial (1st cycle) value after 1000 load cycles (compression to densification at $0.5Hz$). This is likely attributed to a combination of inherent temperature-dependent stiffness of the base material, which was warm to the touch by the end of testing, and possible permanent damage to the sample via local yield in regions of high strain. Cycle frequency was limited to ($0.5Hz$) to prevent inertial effects from influencing force measurements while also limiting the duration of the test.

We quantify dissipation in impact scenarios using the coefficient of restitution CoR, which ranges between 0 (for a perfectly inelastic, fully dissipative impact) and 1 (for a perfectly elastic, zero-dissipation impact):

$$CoR = \frac{v_{out}}{v_{in}} \tag{3}$$

where v_{in} and v_{out} indicate the incident and exit velocity, respectively. The off-vertical components of these velocities are strictly zero in simulation (using prescribed velocity boundary conditions) and in experiment (using a custom impact fixture that constrains motion in all but the vertical dimension), so we use the vertical component of velocity only in calculation of CoR.

Impact tests indicate that impacts on reference foam materials are much more inelastic (2× lower CoR at equivalent ρ^*) than on plate lattices for low-energy impacts (Figure 6B, square marks). At increasing impact energies (which are beyond $\bar{U_{crit}}$ for these foams, see Section 2.3), foam materials respond more elastically. This can be attributed to the material's bulk response being more elastic than the macroscale response of the gyroid foam - once specific impact energy exceeds $\bar{U_{crit}}$, the impact becomes more elastic. By augmenting the experimental dataset with an additional 100 simulations of impact tests (Figure 6B, blue circular marks), a more detailed picture of the plate lattice dissipative response emerges. At low specific impact energies, plate lattice compression remains in the small deformation regime (no buckling occurs), and the lattice responds relatively elastically ($CoR > 0.5$). Above a critical energy, which is the energy required to initiate local elastic buckling of the plate lattice walls, the material becomes more dis-

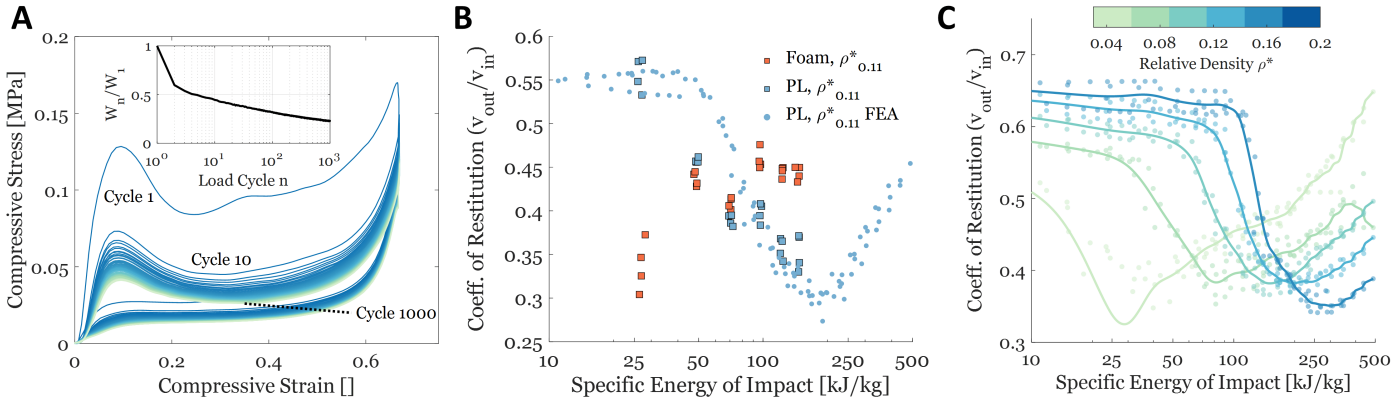

Figure 6: Plate lattice materials dissipate energy (e.g. included area in cyclic load curve, A) during cyclic loading. Repeated loading induces significant softening of the structure, and normalized dissipated energy drops to 25% after 1000 compressions to densification (A). In dynamic testing, low energy impacts excite only linear elastic deformations in plate lattice samples (B), resulting in relatively low energy dissipation (high CoR). Augmenting test data with 100 simulated impacts reveals that as deformation increases at higher impact energies, a larger fraction of that energy is dissipated; this trend reverses beyond a critical impact energy that results in full densification, after which bulk compression in the material leads to increasing CoR. Subscripts on ρ^* indicate relative density. C shows similar behaviors in scans across impact energy at various relative densities; as ρ^* increases, plate lattices dissipate energy effectively (low CoR) across a wider range of impact energies. Solid lines in C show dissipative behavior of plate lattice samples across a range of specific impact energies using a 15-point moving average filter on simulation points.

sipative with increasing impact energy, and the CoR eventually falls to 50% of its initial value. However, beyond a critical impact energy U_{crit}, the material behaves more elastically and CoR begins to increase with additional impact energy (the increase seen above 200 kJ/kg in Figure 6B). This can be attributed to the material's bulk response being much more elastic than the macroscale lattice response. As specific impact energy increases and drives the material beyond the point of densification, bulk effects increasingly and eventually overwhelmingly influence the macroscale lattice response. This trend holds across 800 simulations of impacts on plate lattices with relative density ρ^* ranging from 0.02 to 0.22 (Figure 6C). Denser lattices require more energy to initiate buckling, but also display highly dissipative behavior over a wider range of impact energies - this is a direct result of the impact energy bandwidth increase shown in Figure 4D.

3 Conclusion

This work focuses on the mechanical characterization of additively manufactured plate lattice metamaterials with exceptional specific stiffness and specific impact energy absorption in out-of-plane compression. By leveraging additive fabrication technologies capable of directly writing the sub-mm geometry of these materials, we exceed scaling relationships established for stochastic foam materials. By sacrificing isotropy, we demonstrate near-linear specific stiffness scaling with relative density and increased specific impact energy absorption relative to isotropic plate lattices. Our automated geometry design, additive manufacturing, and simulation toolchain enables continuous and local control over geometric attributes, allowing practitioners to exert precise control over plate lattice metamaterials and to predict their behavior before fabricating. We conduct extensive experimental and numerical testing of plate lattice designs across several orders of magnitude of strainrate, in both prescribed-velocity and prescribed impact energy tests, and demonstrate that plate lattice materials uniformly outperform reference foams in the out-of-plane direction. In comparison to previous investigations of similar plate lattices, we improve energy absorption efficiency by enabling and investigating spatially-varying geometric prebuckling, which improves the energy absorption efficiency by up to 25% relative to prior work.

In fabrication and experimental testing, we were restricted to a narrow range of relative densities limited on the lower end by print nozzle diameter and available test volume, and the upper end by relatively low-force compression testing equipment. It would be informative to experimentally explore lat-

tices across a wider range of relative densities, design regions only accessible via simulation in this work. Similarly, as the thermoplastic polyurethane base material for these plate lattices exhibits marked viscoelastic behavior, exploring their response to higher strainrate loading at equivalent impact energy density could reveal marked performance differences. The impact energy absorbing structures presented here also have application in vibration isolation; future work could characterize their energy dissipation properties over a range of excitation frequencies. A natural extension of this work would be to explore similar metamaterial geometries fabricated from different base materials. In particular, plate lattices made from stiffer, less viscous base material (e.g. aluminum) could yield metamaterials with high impact energy absorption. As base material and geometry changes, future work may examine how transitions between elastic buckling, yield and plastic flow, and brittle fracture impact macroscale absorption performance.

In this work we utilize finite element simulation to explore the design space for a family of plate lattice structures more completely than is tractable using experimental means. However as the geometric complexity of plate lattices scales to include designs with hundreds of thousands or millions of faces, direct numerical simulation poses a bottleneck. Surrogate or reduced order computational models of plate lattice deformation could likely be built to mitigate this barrier to computational design of large scale plate lattice materials, an approach that has proven useful in simulation of beam lattices [51]. Recent work in training neural networks to learn contact-enabled nonlinear continuum mechanics simulations over computational meshes [52] may also be highly applicable accelerating simulation of full-resolution metamaterials.

4 Materials and Methods

Full details on plate lattice design and fabrication, base material characterization, experimental testing, numerical modelling, and mathematical derivations are given in Supplementary Information.

Sample Design and Fabrication

Our custom constructive geometry script allows designers to exert precise, local control over plate lattice geometry and realize designs not previously explored, including those with nonuniform wall thickness, prebuckling magnitude, and cell sizes. In this work we utilize fused filament fabrication (FFF) 3D printing and a soft thermoplastic polyurethane (TPU) elastomer (©*SainSmart*) to fabricate all samples under test. The TPU material chosen for this study has a nominal Shore A hardness of 92, which strikes a balance between being soft enough to enable relatively low-force characterization experiments, and stiff enough to allow robust, repeatable fabrication of many samples with high yield. Samples were fabricated using a commodity FFF 3D printer (Prusa MK3s, *Prusa Research*) fitted with an upgraded direct drive filament extruder designed for higher torque (Bondtech Prusa i3 Upgrade, *Bondtech, AB*) and a high-flowrate nickel-coated brass nozzle with $0.6mm$ orifice diameter (Bondtech CHT, *Bondtech, AB*). Fabrication files were generated for all samples using the open-source slicing program *PrusaSlicer*, with 100% infill and linear extrusion rate of $30mm/s$.

Experimental Testing

A low-force, high-stroke load frame was used for quasistatic mechanical characterization (810E5 All-Electric Dynamic Test Machine, *Test Resources*). In compression tests, a sample was loaded between two parallel aluminum plates with $100mm$ diameter, and the upper plate was lowered at a rate of $0.5mm/s$ ($\dot{\varepsilon} = 10^{-1}s^{-1}$) up to $\varepsilon_{latt} = 0.75$ while vertical displacement of the upper plate and compression force was logged at $1kHz$ (Table 2). All samples were compressed at ambient conditions and allowed to recover for a minimum of $1000s$ between tests to mitigate temperature-dependent stiffness changes and allow sufficient recovery time for long-term viscoelastic effects.

A custom impact fixture was designed and fabricated to characterize dynamic plate lattice behavior, capable of delivering prescribed impact energy and measuring the force reacted by the fixture as well as the sample compression (diagram available in Supplementary Information). The fixture consists of an aluminum carriage with a cantilever impact arm that rides freely on a vertical rail $2m$ in height, and a test plate placed directly below the the impact arm (see Supplemental Information). The user prescribes the impact mass by loading the arm with up to $20kg$ in cast steel plates, and the impact velocity by adjusting the carriage drop height (Table 2).

Immediately before impact, a microprocessor simultaneously triggers the start of load cell signal collection on a data acquisition card (Labjack U6 Pro, ©*Labjack*), and the capture of high speed video on a suitable camera (Phantom v710, ©Vision Research). Position data is extracted from high-speed video using the common visual fiducial system *AprilTag* [53]. In post processing, custom code performs temporal alignment of these signals, yielding synchronized force-displacement data which allows the extraction of dynamic stress-strain curves. All testing is performed at ambient laboratory conditions and samples are allowed to recover for a minimum of $1000s$ between tests to mitigate temperature-dependent stiffness changes and allow recovery from viscoelastic effects.

Numerical Modeling

Simulations were conducted using the nonlinear finite element package *Abaqus* (©Dassault Systemes). All simulations, regardless of loading rate, were performed using the Abaqus dynamic explicit solver, in order to access the general contact algorithm, as in [34, 45]. Coulomb friction is defined at all contact surfaces with a sliding coefficient of friction equal $\mu = 0.75$, imitating real-world conditions where lattice materials may contact plastics, other elastomers, or flesh. A parameter sweep over this coefficient of friction value shows simulations are relatively insensitive to μ so long as it is high enough to prevent nonphysical large-scale sliding on the impact platens. A hyper-viscoelastic constitutive model is implemented to capture the TPU's nonlinear stress-strain relationship and rate-dependent elastic effects, yielding a material model which adequately captures material behavior across a wide range of loading rates (Table 3).

To prevent over-estimation of critical buckling load in numerical analysis of plate lattices with zero geometric prebuckling (designs with perfectly vertical walls), these designs were perturbed in the undeformed configuration by the lowest-energy buckling mode. The eigenmode was extracted using a linear perturbation analysis step and scaled so that the peak displacement magnitude was equal to 10% of the wall thickness, as in [30]. Predictably, designs which include geometric prebuckling ($e^* > 0$) are insensitive to geometric perfections, so this step was omitted.

Numerical and experimental investigations are aimed at obtaining a homogenized macroscale response for various geometries tested. In order to determine the number of unit cells required to adequately recover the macroscale response of plate lattices, a scaling study was performed in which the lattice size was incrementally increased until the quasistatic compression response converged (with a lattice size of 4x4x6 unit cells, see Supplemental Information). Lattice aspect ratio was controlled via geometric parameters w_c and h_c to ensure a progressive buckling collapse mechanism, rather than macroscale buckling.

Table 2: Quasistatic and Dynamic Test Fixtures

	DMA	Impact Fixture
Crosshead Velocity (m/s)	5e-5-5e-1	1.0 - 3.5
Impact Mass (kg)	N/A	3-17
Load Capacity (N)	720	9800
Load Collection (kHz)	1	12.5
Position Collection (kHz)	1	25

Table 3: Ogden-Prony hyper-viscoelastic material model

	Ogden Model			Prony Model		
	μ_i (MPa)	α_i	D_i (MPa)	g_i	τ_i (s)	K_i (MPa)
1	0.028	4.247	0	*0.503*	0.001	0
2	7.812	-2.079	0	*0.186*	0.01	0
3	-	-	-	*0.018*	0.1	0

ASTM dogbone testing; *estimated from impact tests*; assumed

Supporting Information

Supporting Information is available from the Wiley Online Library or from the author.

Author Information

Lawrence Smith researches additive manufacturing, soft robotics, and numerical simulations of soft matter at the University of Colorado Boulder. He holds an M.S. and Ph.D. in Mechanical Engineering from the University of Colorado Boulder and a B.S. in Mechanical Engineering from California Polytechnic University, San Luis Obispo. Email: *lasm4254@colorado.edu*

Robert MacCurdy's research interests include Modular Robotics, Additive Manufacturing, Digital Materials, Heuristic Optimization and Bio-instrumentation. He holds an M.S. and Ph.D. in Mechanical Engineering, as well as a B.S. in Electrical Engineering from Cornell University, and a B.A. in Physics from Ithaca College. Email: *maccurdy@colorado.edu*

Brandon Hayes investigates additive manufacturing and the fundamentals and applications of multiphase fluid flows at the University of Colorado Boulder. He holds a B.S. in biomedical engineering and microelectronics engineering from Rochester Institute of Technology and a M.S. in mechanical engineering from the University of Colorado Boulder. Email: *brandon.Hayes@colorado.edu*

Kurtis Ford is a principal member of technical staff at Sandia National Laboratories. His research interests have centered around the imperfection sensitivity of buckling, highly flexible beams, fracture in thin coatings, mechanical modeling of welds, additive manufacturing, brittle failure, iso-geometric analysis, crash analysis, digital twin, coupled electrical-mechanical systems, micro-mechanical systems and nonlinear viscoelasticity of epoxy thermosets and inorganic glass. Email: *krford@sandia.gov*

Elizabeth Smith is a R&D mechanical engineer at Sandia National Laboratories. She received a masters degree in Civil Engineering from Imperial College in London. Her interests include modeling and simulation of dynamic environments, blast physics, and fracture mechanics in brittle materials. Email: *edsmith@sandia.gov*

David Flores is a R&D Department manager at Sandia National Laboratories, where he has worked for 14 years. He received a masters degree in Mechanical Engineering from Stanford, and his interests include systems analysis, structural and system fragility, and probabilistic risk assessment. Email: *djflore@sandia.gov*

Table of Contents

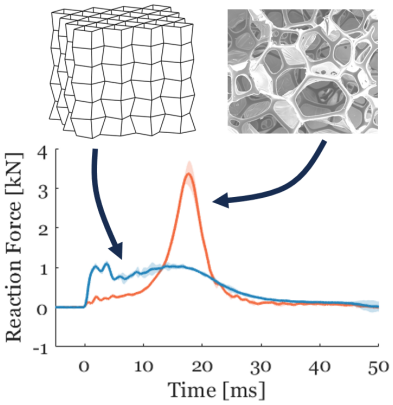

Metamaterials with outstanding impact mitigation performance and unparalleled geometric tailorability enable geometry- and impact energy-specific impact energy absorption solutions.

References

[1] M. F. Ashby, *Philosophical Transactions of the Royal Society A: Mathematical, Physical and Engineering Sciences* **2006**, *364*, 1838 15.

[2] S. J. Yeo, M. J. Oh, P. J. Yoo, *Advanced Materials* **2019**, *31*, 34 1.

[3] B. Song, W. Chen, T. Yanagita, D. J. Frew, *Composite Structures* **2005**, *67*, 3 SPEC.ISS. 279.

[4] M. Shinde, I. E. Ramirez-Chavez, D. Anderson, J. Fait, M. Jarrett, D. Bhate, *Journal of Manufacturing and Materials Processing* **2022**, *6*, 6.

[5] J. Zhang, M. F. Ashby, *International Journal of Mechanical Sciences* **1992**, *34*, 6 475.

[6] G. Gruenbaum, J. Miltz, *Journal of Applied Polymer Science* **1983**, *28*, 1 135.

[7] M. Avalle, G. Belingardi, R. Montanini, *International Journal of Impact Engineering* **2001**, *25*, 5 455.

[8] A. H. Brothers, D. C. Dunand, *Materials Science and Engineering A* **2008**, *489*, 1-2 439.

[9] Y. Hangai, K. Takahashi, T. Utsunomiya, S. Kitahara, O. Kuwazuru, N. Yoshikawa, *Materials Science and Engineering A* **2012**, *534* 716.

[10] R. Maccurdy, R. Katzschmann, Y. Kim, D. Rus, In *Proceedings - IEEE International Conference on Robotics and Automation*, volume 2016-June, ISBN 9781467380263, ISSN 10504729, **2016** 3878–3885, URL http://robertmaccurdy.com/docs/2016_MacCurdy-PrintableHydraulics-Amethodforfabricating.pdf.

[11] P. Qiao, M. Yang, F. Bobaru, *Journal of Aerospace Engineering* **2008**, *21*, 4 235.

[12] C. I. Hammetter, R. G. Rinaldi, F. W. Zok, *Journal of Applied Mechanics, Transactions ASME* **2013**, *80*, 4 1.

[13] R. Gümrük, R. A. Mines, *International Journal of Mechanical Sciences* **2013**, *68* 125.

[14] T. Tancogne-Dejean, D. Mohr, *International Journal of Solids and Structures* **2018**, *138* 24.

[15] C. Bonatti, D. Mohr, *International Journal of Plasticity* **2017**, *92* 122.

[16] T. Tancogne-Dejean, X. Li, M. Diamantopoulou, C. C. Roth, D. Mohr, *Journal of Dynamic Behavior of Materials* **2019**, *5*, 3 361.

[17] C. Bonatti, D. Mohr, *Journal of the Mechanics and Physics of Solids* **2019**, *122* 1.

[18] T. Tancogne-Dejean, M. Diamantopoulou, M. B. Gorji, C. Bonatti, D. Mohr, *Advanced Materials* **2018**, *30*, 45 1.

[19] C. Bonatti, D. Mohr, *Acta Materialia* **2019**, *164* 301.

[20] S. A. Hassanieh, A. Alhantoobi, K. A. Khan, M. A. Khan, *Polymers* **2021**, *13*, 22.

[21] L. Valdevit, S. W. Godfrey, T. A. Schaedler, A. J. Jacobsen, W. B. Carter, *Journal of Materials Research* **2013**, *28*, 17 2461.

[22] M. G. Lee, J. W. Lee, S. C. Han, K. Kang, *Acta Materialia* **2016**, *103* 595.

[23] T. Tancogne-Dejean, D. Mohr, *International Journal of Mechanical Sciences* **2018**, *141*, March 101.

[24] I. Maskery, N. T. Aboulkhair, A. O. Aremu, C. J. Tuck, I. A. Ashcroft, R. D. Wildman, R. J. Hague, *Materials Science and Engineering A* **2016**, *670* 264.

[25] S. R. Bates, I. R. Farrow, R. S. Trask, *Materials and Design* **2019**, *162* 130.

[26] R. D. Hussein, D. Ruan, G. Lu, I. Sbarski, *Composite Structures* **2016**, *140* 166.

[27] W. Goldsmith, J. L. Sackman, *International Journal of Impact Engineering* **1992**, *12*, 2 241.

[28] L. Aktay, A. F. Johnson, B. H. Kröplin, *Engineering Fracture Mechanics* **2008**, *75*, 9 2616.

[29] Z. Wang, H. Tian, Z. Lu, W. Zhou, *Composites Part B: Engineering* **2014**, *56* 1.

[30] J. Fang, G. Sun, N. Qiu, T. Pang, S. Li, Q. Li, *International Journal of Solids and Structures* **2018**, *135* 1.

[31] I. Maskery, N. T. Aboulkhair, A. O. Aremu, C. J. Tuck, I. A. Ashcroft, *Additive Manufacturing* **2017**, *16* 24.

[32] W. Y. Jang, S. Kyriakides, *International Journal of Solids and Structures* **2009**, *46*, 3-4 635.

[33] N. Triantafyllidis, M. W. Schraad, *Journal of the Mechanics and Physics of Solids* **1998**, *46*, 6 1089.

[34] S. Townsend, R. Adams, M. Robinson, B. Hanna, P. Theobald, *Materials and Design* **2020**, *195* 108930.

[35] S. R. Bates, I. R. Farrow, R. S. Trask, *Materials and Design* **2016**, *112* 172.

[36] S. Higuera, R. Miralbes, D. Ranz, *Mechanics of Advanced Materials and Structures* **2021**, *0*, 0 1.

[37] B. Song, W. Y. Lu, C. J. Syn, W. Chen, *Journal of Materials Science* **2009**, *44*, 2 351.

[38] G. C. Jacob, J. F. Fellers, S. Simunovic, J. M. Starbuck, *Composite Materials* **2002**, *36*, 7 813.

[39] S. Cui, R. L. Harne, *International Journal of Solids and Structures* **2018**, *135* 197.

[40] G. Constantinides, C. A. Tweedie, N. Savva, J. F. Smith, K. J. Vliet, *Experimental Mechanics* **2009**, *49*, 4 511.

[41] B. Song, K. Nelson, *Latin American Journal of Solids and Structures* **2015**, *12*, 9 1790.

[42] A. L. DeMarco, D. D. Chimich, J. C. Gardiner, R. W. Nightingale, G. P. Siegmund, *Accident Analysis and Prevention* **2010**, *42*, 6 1778.

[43] K. N. Long, C. M. Hamel, R. Waymel, D. Bolintineanu, E. Quin, S. Kramer **2020**.

[44] P. Vuyk, R. L. Harne, *Extreme Mechanics Letters* **2020**, *37* 100682.

[45] R. Adams, S. Townsend, S. Soe, P. Theobald, *Materials and Design* **2022**, *213* 110368.

[46] S. Shan, S. H. Kang, J. R. Raney, P. Wang, L. Fang, F. Candido, J. A. Lewis, K. Bertoldi **2015**.

[47] C. Luo, C. Chung, N. A. Traugutt, C. M. Yakacki, K. N. Long, K. Yu, *ACS Applied Materials and Interfaces* **2021**, *13*, 11 12698.

[48] A. Schoen, *Electronics Research Center* **1970**.

[49] G. Boschetti, R. Caracciolo, D. Richiedei, A. Trevisani, *Mechanical Systems and Signal Processing* **2013**, *34*, 1-2 116.

[50] A. P. Garland, K. M. Adstedt, Z. J. Casias, B. C. White, W. M. Mook, B. Kaehr, B. H. Jared, B. T. Lester, N. S. Leathe, E. Schwaller, B. L. Boyce, *Extreme Mechanics Letters* **2020**, *40* 100847.

[51] A. E. Gongora, K. L. Snapp, R. Pang, T. M. Tiano, K. G. Reyes, E. Whiting, T. J. Lawton, E. F. Morgan, K. A. Brown, *Matter* **2022**, *5*, 9 2829.

[52] T. Pfaff, M. Fortunato, A. Sanchez-Gonzalez, P. W. Battaglia **2020**, 1–18.

[53] E. Olson, *Proceedings - IEEE International Conference on Robotics and Automation* **2011**, 3400–3407.